Chemical Engineering Journal 146 (2009) 456–465

Contents lists available at ScienceDirect

Chemical Engineering Journal

journal homepage: www.elsevier.com/locate/cej

Production of TiO_2 nanoparticles with controlled characteristics by means of a Vortex Reactor

Daniele L. Marchisio*, Federica Omegna, Antonello A. Barresi

Dipartimento di Scienza dei Materiali e Ingegneria Chimica, Politecnico di Torino, C.so Duca degli Abruzzi 24, 10129 Torino, Italy

ARTICLE INFO

Article history:
Received 18 March 2008
Received in revised form 13 October 2008
Accepted 17 October 2008

Keywords:
Sol–gel
Titanium dioxide
Mixing
Titanium alkoxide
Computational fluid dynamics
Vortex Reactor
Population balance modelling

ABSTRACT

In this work titanium dioxide nanoparticle formation and evolution via the sol–gel route is investigated. Alcoholic solutions of titanium tetra-isopropoxide and water are mixed in a Vortex Reactor, where the mixing time can be accurately controlled by manipulating the inlet flow rates. Particle synthesis is carried out in operating conditions ranging from poor to excellent mixing performances and the effect of mixing on the formation of titanium dioxide nanoparticles and on their evolution is investigated from the modelling and the experimental view points. Experiments are in fact interpreted by using a simple population balance model and mixing in the reactor is accurately described by a computational fluid dynamics model based on the calculation of characteristics mixing times. Results show that particle formation is strongly influenced by mixing and that particle aggregation/condensation occurs in the reaction limited regime.

1. Introduction

Titanium dioxide is widely used as white pigment, and its optical properties are governed by refractive index and grain size. In fact, micrometric particles are generally opaque for visible light, whereas smaller nano-sized particles are transparent to visible light but still UV blocker [1]. Another important property is related to the fact that titanium dioxide is a super-hydrophilic material, thank to the almost null contact angle with water. Therefore it can be used to develop surfaces easy to clean and when a natural source of water exists, it can be used to develop self-cleaning surfaces.

Titanium dioxide is moreover well know for its ability to generate, when exposed to light, high mobility electrons and holes, that in turn are able to promote chemical reactions, resulting in a material with unique photo-catalytic properties [2,3]. The ability of titanium dioxide to degrade several organic compounds has been widely studied and it has been shown that this material can be profitably used to treat liquid and gaseous waste streams. Kinetic studies have shown that the photo-catalytic activity of titanium dioxide is greatly influenced by the crystalline form, although controversial results are reported in the literature. For example, some authors state that anatase works better than rutile [4,5], others found the best photo-catalytic activity for rutile [6–8], and some others detected synergistic effects in the photocatalytic activity for anatase-rutile mixed phases [9–11]. Besides, recently it was demonstrated that photo-activity in organics degradation depends on the phase composition and on the oxidizing agent; for example, when the performance of different crystalline forms is compared, it turns out that rutile shows the highest photo-catalytic activity with H_2O_2 whereas anatase with O_2 [12,13]. Naturally the ability of titanium dioxide particles to degrade organic compounds depends also on the size of the particles, since small particles offer larger surface areas [14]. For its properties titanium dioxide has been recently implemented as filler for inorganic materials (plaster, mortar, and concrete [15]) and organic polymeric materials [16,17]. Also for these applications particle size is crucial, since only by using nano-sized fillers, materials with synergic properties, rather than compromising ones, are obtained. The improved properties of nano-composites are due to the large interfacial area offered by the nano-scale filler that controls the degree of interaction between the filler and the matrix [18].

Many processes for the production of titanium dioxide particles exist, namely flame aerosol synthesis [19], hydrothermal synthesis [20–23] and sol–gel synthesis [24]. Flame aerosol synthesis presents the main advantage of being easily scalable to the industrial level, but presents all the disadvantages of high temperature syntheses. Hydrothermal synthesis is instead particularly interesting for it directly produces a crystalline powder, without the need of resorting to a final calcination step, which is instead required in the sol–gel process. However the lack of knowledge of the chemical

* Corresponding author.
E-mail address: daniele.marchisio@polito.it (D.L. Marchisio).

1385-8947/$ – see front matter © 2008 Elsevier B.V. All rights reserved.
doi:10.1016/j.cej.2008.10.031

equilibria of the species in solution and of the kinetics of nucleation and growth of the different phases, makes it difficult to control the overall process. The sol–gel route is at the moment the most common and promising one at the laboratory scale. It is based on the reaction between some precursor (e.g., titanium alkoxide) and water that are usually mixed as alcoholic solutions, with the addition of some catalysts to control the reaction (e.g., hydrochloric acid).

After mixing a fast hydrolysis reaction occurs:

$$M(OR)_n + H_20 \rightarrow M(OR)_{n-1}(OH) + ROH$$

followed by de-hydration:

$$2\,M(OR)_{n-1}(OH) \rightarrow M_2O(OR)_{2n-2} + H_2O$$

and de-alcoholation:

$$M(OR)_n + M(OR)_{n-1}(OH) \rightarrow M_2O(OR)_{2n-2} + ROH$$

resulting in the following overall reaction [25]:

$$M(OR)_n + \tfrac{n}{2}H_2O \rightarrow MO_{n/2} + n\,ROH$$

Water consumption measurements [26,27] seem to show that in the case of many titanium alkoxides, hydrolysis is generally faster than condensation, and that the first hydrolysis step corresponds to the creation of a supersaturated solution. From this supersaturated solution, after nucleation (i.e., formation of small nuclei of hydrolysed monomers) and molecular growth (addition of a single monomer to the nuclei), a colloidal suspension (i.e., sol) is generated, that subsequently, because of collisions due to Brownian motions, further condensation, and depending on the inter-particle potential, aggregates and may be transformed into a gel [28]. Although generally hydrolysis is faster than condensation their relative rates still depend on the operating parameters during particle formation, and under particular operating conditions (e.g., initial concentration of alkoxide in the alcohol solution, water to alkoxide ratio, concentration and nature of the catalyst, pH, etc.) hydrolysis and condensation can be almost simultaneous, leading immediately to the formation of a gel. Generally the formation of the gel is followed by a drying stage, that usually involves further condensation, and by a calcination step, where the amorphous material is transformed in crystalline particles. The final calcination step is crucial, because of the difficulties in controlling the crystalline form (anatase versus rutile) and in avoiding undesirable phenomena, such as grain growth with reduction of the superficial area [29].

Although the sol–gel process has been known almost for a century and some of the most important chemical aspects have been cleared, there exists room for improvement for individuating synthesis conditions that result in a powder with improved properties, when compared with commercial products available at the moment. Moreover up-scaling the process from the laboratory to the industrial scale is still a complex problem of difficult solution. The main issue stands in the fact that mixing plays a big role but its effects are usually underestimated, as proven by the qualitative statements (e.g., add dropwise or mix vigorously) with which ideal mixing conditions are usually identified. Mixing (usually turbulent) plays a very important role in the initial formation of the sol and as a consequence in the subsequent gelation process. In order to evaluate the relative importance of the different phenomena involved, it is crucial to quantify the characteristic time-scales for mixing, hydrolysis, and condensation/aggregation. Turbulent mixing occurs at several time- and length-scales; it starts on a scale of the same order of magnitude of the equipment in which the process occurs and it ends on a very small scale (Batchelor scale), that is determined by the fluid transport properties (i.e., viscosity and diffusivity) and by turbulence intensity (i.e., turbulence dissipation rate) [30]. The characteristic mixing time is therefore given by the summation of the time required to reduce the scale of segregation from the macro-scale (macro-mixing) down to the molecular scale (micro-mixing) and can be determined by experimental techniques [31] or mathematical models based on computational fluid dynamics (CFD) [32,33]. The characteristic time for hydrolysis is usually related to the induction time, namely the time required for the formation of a visible solid phase [34] whereas the characteristic time for aggregation/condensation is evaluated based on the local particle concentration and on the aggregation kernel [35].

A number of investigations show that the ratio between these characteristic time-scales controls the final characteristics of the solid product. For example, in many particle formation processes the initial particle size is determined by the relative values of mixing and particle formation time-scales, and only if mixing is very fast ultra fine particles are formed [36–39] whereas in the case of sol–gel processes only some preliminary results were obtained [40]. Moreover, the size of the initial particles and their local concentration control the formation of the gel affecting its most important features, such as its rheological and fractal properties. The aggregation process, leading to the formation of the gel, is often studied by resorting to the Smoluchowski theory [41], by adopting population balance models (PBM) [42,43] and is driven by Brownian motions (i.e., perikinetic aggregation) [28].

The main objective of this work is to quantitatively investigate the effect of mixing on TiO_2 nanoparticles formation and evolution. To this end a specific sol–gel process is considered, based on the reaction between titanium tetra-isopropoxide and water in isopropanol. The effect of the different operating parameters on this sol–gel process was recently studied from the experimental point of view [44]. The experimental campaign was conducted by means of a statistical analysis (i.e, Design of Experiment) and results showed that the mixing rate strongly affects the final Particle Size Distribution (PSD). However, a number of issues related to the CFD simulation of mixing dynamics, the quantitative analysis of the resulting mixing time-scales, as well as the quantitative investigation of the final aggregation/condensation process were not discussed. All these aspects are instead investigated and discussed in details in this work. In fact, CFD is used here to quantify the mixing time and moreover the evolution of the formed particles is treated with a PBM in order to extract useful kinetics parameters. This investigation is carried out in a passive mixer, namely the Vortex Reactor, where simply changing the inlet flow rates of the reactant solutions the characteristic mixing time can be easily manipulated, as demonstrated in similar works [45,46]. Different titanium dioxide samples are prepared under different mixing conditions and their time evolution is tracked with time, since some of them result in stable sols, whereas some others aggregate and evolve in bigger clusters or degenerate into gels. Therefore the effect of mixing is quantified not only on the nanoparticles immediately formed after the first stages of hydrolysis and condensation, but also on the final particulate products obtained from the overall sol–gel process.

The manuscript is structured as follows: firstly the equations governing mixing dynamics and nanoparticle evolution are presented and discussed. Then the experimental set up, numerical details and operating conditions are described. Eventually the experimental and modelling results are presented and some relevant conclusions are drawn.

2. Governing equations

Turbulent mixing of two (or more) fluid streams into a chemical reactor is often described in terms of the mixture fraction ξ. This

quantity is a normalized inert scalar concentration that is assumed equal to one in one feed stream and zero in the other, and therefore represents the amount of fluid coming from one inlet with respect to the other. When the Reynolds-averaged Navier–Stokes (RANS) approach is used the problem is described in terms of Reynolds-averaged mixture fraction $\langle\xi\rangle$ whose transport equation reads as follows:

$$\frac{\partial\langle\xi\rangle}{\partial t} + \langle u_j\rangle\frac{\partial\langle\xi\rangle}{\partial x_j} - \frac{\partial}{\partial x_i}\left[(\Gamma+\Gamma_t)\frac{\partial\langle\xi\rangle}{\partial x_i}\right] = 0, \tag{1}$$

where the fluid is assumed to be incompressible (i.e., constant density flow), where Γ and Γ_t are the molecular and turbulent diffusion coefficients, respectively, and where the source term is null since the mixture fraction is a non-reacting scalar. It is important to highlight here that the solution of Eq. (1) and the knowledge of the mixture fraction values throughout the reactor is very useful, since it contains information on the mixing efficiency at the macroscopic level. Moreover, although the mixture fraction is a non-reacting scalar it is very much used also for the description of reacting systems. In fact, when the chemical reactions involved are infinitely fast, mixing is the limiting step for their completion, and therefore the mixture fraction alone suffices to completely describe the reacting systems. Moreover, when the chemical reactions are characterized by finite-rates the reacting system is still described in terms of the mixture fraction and in terms of additional reaction progress variables.

The turbulent diffusion coefficient appearing in Eq. (1) is calculated as follows:

$$\Gamma_t = \frac{C_\mu}{Sc_t}\frac{k^2}{\varepsilon} \tag{2}$$

where $Sc_t \cong 0.7/1.0$ is the turbulent Schmidt number and C_μ is a numeric constant equal to 0.09. The turbulent kinetic energy k and the turbulent kinetic energy dissipation rate ε are usually calculated by resorting to a two-equation model (e.g., standard $k-\varepsilon$, RNG $k-\varepsilon$, realizable $k-\varepsilon$, standard and shear-stress-transport $k-\omega$) or by resorting to more sophisticated closures such as the Reynolds Stress Model (RSM) [47]. It is interesting to highlight that some of these models appear to be more indicated to the treatment of swirling flows as in the case of the Vortex Reactor. The Realizable $k-\varepsilon$ contains for example a special correction for swirling flows, and the RSM is also known to perform well for such flows. However, in order to discern among the possible modelling choices, detailed experimental data on the velocity and turbulent fields are needed.

When mixing in a chemical reactor is very efficient the mixture fraction $\langle\xi\rangle$ will assume almost everywhere in the reactor a constant value, corresponding to complete mixing conditions (i.e., $\bar{\xi}$). Based on this quantity, a large-scale variance is defined:

$$\langle\xi'^2\rangle_L = \left(\langle\xi\rangle - \bar{\xi}\right)^2, \tag{3}$$

equal to zero where mixing is complete and greater than one in regions where macro-scale gradients are still present. Although it is not directly solved, it is useful to derive the transport equation for this quantity, that reads as follows [32]:

$$\frac{\partial\langle\xi'^2\rangle_L}{\partial t} + \langle u_j\rangle\frac{\partial\langle\xi'^2\rangle_L}{\partial x_j} - \frac{\partial}{\partial x_i}\left[(\Gamma+\Gamma_t)\frac{\partial\langle\xi'^2\rangle_L}{\partial x_i}\right] = -2\Gamma_t\frac{\partial\langle\xi\rangle}{\partial x_i}\frac{\partial\langle\xi\rangle}{\partial x_i}, \tag{4}$$

where as it is possible to see the large scale variance is dissipated by turbulent diffusion (negative term on the right-hand side) whereas it has no generation term, since the large-scale variance is generated by feeding the reactants in different inlets.

This large-scale variance is transported to smaller time- and length-scales thank to turbulent diffusion, and generates what is called the small-scale variance. This quantity represents the segregation (or variance) at the molecular level and is defined as the average mixture fraction fluctuations ξ', around the average value $\langle\xi\rangle$:

$$\langle\xi'^2\rangle_s = \langle(\xi-\langle\xi\rangle)^2\rangle = \frac{1}{\Delta t}\int_t^{t+\Delta t}(\xi-\langle\xi\rangle)^2\,dt, \tag{5}$$

and its transport equation reads as follows [21]:

$$\frac{\partial\langle\xi'^2\rangle_s}{\partial t} + \langle u_j\rangle\frac{\partial\langle\xi'^2\rangle_s}{\partial x_j} - \frac{\partial}{\partial x_i}\left[(\Gamma+\Gamma_t)\frac{\partial\langle\xi'^2\rangle_s}{\partial x_i}\right] = 2\Gamma_t\frac{\partial\langle\xi\rangle}{\partial x_i}\frac{\partial\langle\xi\rangle}{\partial x_i} - 2\frac{C_\phi}{2}\frac{\varepsilon}{k}\langle\xi'^2\rangle_s, \tag{6}$$

where as it is possible to see the generation of small-scale variance equals the dissipation of large-scale variance; as already reported, segregation is generated originally from feeding the reactants in two separate feed streams, then is transported to smaller length-scales, and is finally dissipated at the molecular level through molecular mixing (see the last term on the right-hand side of Eq. (6)). The micro-mixing rate is usually written in terms of the integral time scale of turbulence (i.e., k/ε) and of the scalar-to-turbulence ratio C_ϕ, that is equal to two for fully turbulent flows, and can be calculated accurately by using the interpolation formula proposed by Liu and Fox [32], valid for Schmidt numbers much higher than one.

Based on these equations it is possible to calculate the overall mixing time as the summation of the time required to destroy macro-scale gradients, also known as macro-mixing time, and the time required to destroy micro-scale gradients, also known as micro-mixing time:

$$t_m = \frac{\langle\xi'^2\rangle_L}{2\Gamma_t(\partial\langle\xi\rangle/\partial x_i)(\partial\langle\xi\rangle/\partial x_i)} + \frac{1}{C_\phi}\frac{k}{\varepsilon}, \tag{7}$$

where the first and the second term are the macro- and micro-mixing characteristic times respectively

As far as particle formation and evolution is concerned in sol–gel processes traditionally two steps are identified. In the first step particles are nucleated and grow from addition of single molecules, forming almost instantaneously a suspension of ultra-fine particles, referred to as sol. Then, depending on the operating conditions, this sol can aggregate evolving into a gel or can remain stable. The first step (i.e., particle formation) is very fast and is generally assumed to coincide with hydrolysis; during this step some water and most of the precursor are consumed. The second step is instead much slower and its rate is usually controlled by condensation. Since this second step is much slower than mixing, as shown by our previous work [35], the population balance equation can be simplified as follows:

$$\frac{\partial n(v;t)}{\partial t} = \underbrace{\frac{1}{2}\int_0^v \beta(v-\epsilon,\epsilon)n(v-\epsilon;t)n(\epsilon;t)d\epsilon}_{(1)} - \underbrace{n(v;t)\int_0^\infty \beta(v,\epsilon)n(\epsilon;t)d\epsilon}_{(2)}, \tag{8}$$

where $n(v;t)$ is the number density function in terms of the particle volume (or mass), identifying the number of particles having volume (or mass) in between v and $v+dv$; $\beta(v,\epsilon)$ is the volume-based aggregation kernel that describes the frequency that particles with volume v and ϵ collide to form a particle of volume $v+\epsilon$. As concerns the terms on the right-hand side of Eq. (8) they have the

following meaning. The first term (1) represents the rate of birth of particles of volume v due to aggregation of smaller particles, whereas the second term (2) is the rate of death of particles of volume v due to aggregation with other particles. The aggregation kernel, describing the frequency that particle collide and stick, is usually evaluated by combining two contributions, the first one taking into account the frequency of aggregation due to Brownian motions (i.e., diffusion limited aggregation, DLA) and the second one taking into account the frequency of aggregation due to condensation (i.e., reaction limited aggregation, RLA). Soloviev et al. [48] has shown that DLA cannot be responsible for the gelation time required in many sol–gel processes, because in this range of operating conditions it would result in very fast aggregation in comparison with what is experimentally observed. The RLA regime has therefore been suggested resulting in the following aggregation kernel:

$$\beta(v, \epsilon) = k_0 c_W^p, \tag{9}$$

where k_0 is the kinetic constant of the controlling condensation reaction, c_W is the water residual concentration after hydrolysis, and p is an exponent calculated as follows:

$$p = 2n - k + 1, \tag{10}$$

where n is the number of functional groups available for condensation (after hydrolysis), whereas k is the controlling condensation step, with $1 < k \leq n$. For example, if four functional groups are available and after hydrolysis one group has reacted, n results to be equal to three; if the condensation of the second group is the controlling one then $p = 5$ whereas if the condensation of the third group is controlling then $p = 4$, and so on.

As it is seen from Eq. (9) the aggregation kernel does not depend on particle volume and for this reason this equation can be solved analytically by using the method of moments. The final time evolution of the moment of zero order (the total particle number density, N) results in what follows:

$$N(t) = N_0 - \frac{k_0 c_W^p c_{Ti}^2}{2} t, \tag{11}$$

where $N(t)$ represents the time evolution of the total number of titanium dioxide particles of all size per unit volume, c_W is the water residual concentration after hydrolysis, N_0 is the total particle number density after hydrolysis (before condensation) and c_{Ti} is the titanium concentration is the solution. This model describes therefore particle formation as instantaneous and resulting in the formation of N_0 particles per unit volume and it predicts a linear decrease with time of the total particle number density $N(t)$ until gelation occurs; the gelling time corresponds to the time required to aggregate all the primary particles into one single particle, and therefore can be easily calculated from Eq. (11).

3. Operating conditions and numerical details

In this work titanium dioxide particle formation has been investigated from the experimental and modelling viewpoints. Titanium dioxide was synthesized by mixing a solution of micro-filtered water and reagent grade isopropanol with a solution of titanium tetra-isopropoxide (TTIP) in isopropanol. The solutions were prepared separately under nitrogen flux to control the alkoxide reactivity with humidity and moreover hydrochloric acid (HCl) was added at different initial concentrations as a hydrolysis catalyst and de-agglomeration agent. Equal volumes of reactant solutions (i.e., 100 ml) were mixed at equal flow rates at 30 ° C in a VR and then for both configurations the solutions exiting the reactor were collected in a small vessel thermostated at 30 ° C and gently stirred. The VR used in this work is constituted by a cylindrical chamber of 12 mm in diameter and 3 mm in height; two reactant streams are fed tangentially at opposite sides of the reactor through two pipes of 3 mm of diameter, whereas the mixed solutions leave the reactor from the bottom through an outlet pipe of 3 mm of diameter. Because of the size of the reactor wall effects are very important, as reflected by the choice of the wall treatment in the CFD simulations.

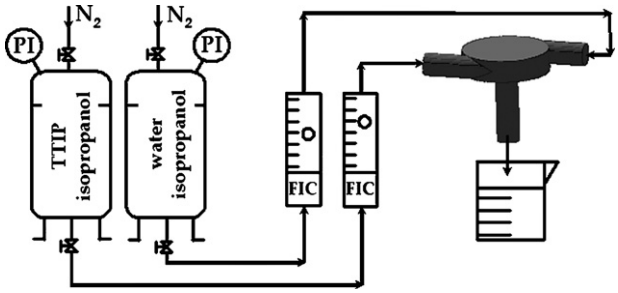

Fig. 1. Sketch of the experimental set-up.

The reactant solutions were stored in two small identical vessels, then pressurized at 3 bar with analytical grade nitrogen; the inlet flow rates were manipulated with two rotameters in the range from 10 to 400 ml/min. A sketch of the experimental apparatus is reported in Fig. 1.When the inlet flow rates of the two reactant solutions are varied from 10 to 400 ml/min, the mean residence time in the mixer approximately changes from about 5–0.05 s and the flow field is completely modified, moving from low turbulence and very poor mixing performances, to highly turbulent conditions with very rapid and efficient mixing dynamics, as it will be shown later.

The characterization of the particulate systems obtained in the different experiments is carried out assuming an instantaneous formation of solid particles and a subsequent slow aggregation/condensation process. The particle size distribution (PSD) of the sol instantaneously obtained after mixing was measured immediately by dynamic light scattering (DLS) with Malvern Nano ZS90 providing reliable information in the size range from 1 to 6000 nm; the PSD was then used to determine the mean particle size (d_{mean}) and the initial total particle number density (N_0) simply assuming that all the TTIP had reacted immediately. Then the PSD is tracked with time with regular measurements, approximately every 3 to 5 min depending on the operating conditions. The suspensions were then filtered with a micro-filtration system (Sartorius P.47, 200 ml) using a 0.1 μm membrane, dried at 120 °C, washed with a solution of 0.02 % in weight of isopropanol and poly-acrylic-acid (PAA 2000, Aldrich) and after 15 min of ultrasonic treatment the suspension was filtered again. The ultrasonic treatment was carried out in order to break aggregates that might have been formed during filtration. The resulting powders were eventually calcined at 400 ° C for 2 h. Scanning electron microscopy (SEM) and field emission scanning electron microscopy (FESEM) were carried out before and after thermal treatments.

Different experiments were carried out by varying the operating conditions during synthesis and by ranging the initial TTIP concentration in the isopropanol solution (c_{Ti}) between 0.1 and 2 mol/l, the ratio between the water and the TTIP concentrations in their initial solutions (W), also known as hydrolysis ratio, was varied between 1 and 4, whereas the ratio between the hydrochloric acid and the TTIP concentrations (H) was kept in between 0.25 and 0.5. The FR of the two solutions were kept at equal values and were varied between 10 and 400 ml/min, resulting in Reynolds numbers in the inlet jets (Re_j) ranging between 40 and 1000. Each experiment was repeated twice (and in some cases three times) to assess the syn-

Table 1
Summary of the operating conditions of experiments

c_{Ti}	W	H	FR
0.1	2	0.25	110
0.5	2	0.25	110
0.5	2	0.5	110
0.5	4	0.25	110
0.5	4	0.5	110
1	2	0.25	3
1	2	0.25	83
1	2	0.25	110
1	2	0.25	220
1	2	0.25	330
1	2	0.5	110

thesis and characterization protocol reproducibility. A summary of the different experiments performed is reported in Table 1.

Mixing in the reactor was investigated by running CFD simulations with the commercial code Fluent 6.3.26. Different computational grids were tested, and after subsequent refinements a grid-independent solution was obtained. The final grid contained about 200,000 computational cells. Simulations in turbulent conditions were run using the so-called RANS approach, by employing the realizable k– ε turbulence model and non-equilibrium wall functions for the near wall treatment. Other turbulence models and near wall treatments were tested, but the use of more sophisticated approaches did not affect very much the final predictions. In order to avoid the insidious effects of numerical diffusion higher order discretization schemes were employed (i.e., third order scheme). Due to the very wide range of operating conditions investigated, some of the simulations were run at very low jet Reynolds, corresponding to very low turbulence. Under these conditions the RANS approach is well known to fail in predicting accurately the velocity field in the reactor and the mixing dynamics. Moreover the lack of experimental data concerning the velocity field inside the reactor does not allow for a direct validation of CFD predictions. Therefore, although the absolute values of the mixing times extracted should be treated with great caution, this CFD analysis is still valid and very useful to estimate trends and orders of magnitude.

The flow field was first simulated assuming that the two reactant solutions (mainly constituted by isopropanol) were characterized by identical physical properties, namely a density of 0.785 kg/l and a viscosity of 2 cP. The transport equations for the mean mixture fraction (see Eq. (1)) and for the mixture fraction variance (see Eq. (6)) were instead solved by introducing them as user defined scalars. The boundary conditions were such that the mean mixture fraction was equal to one in one inlet and equal to zero in the other one, whereas the mixture fraction variance was set equal to zero in both inlets since it is not defined in pure feed streams. With the same subroutines the global mixing time was evaluated by solving Eq. (7).

4. Results and discussion

As it has been reported each experiment has been repeated twice (and in some cases three times) to verify the reproducibility of the synthesis and characterization protocol. In Fig. 2 the PSD of the three different samples prepared under the same operating conditions is reported and as it is possible to see the three curves are quite close. The overall reproducibility of the synthesis and characterization protocol resulted in standard deviation for the mean particle size of about 15 to 20%.

The effect of the initial concentration of titanium alkoxide (c_{Ti}) is reported in Fig. 3; as it is possible to see an increase in the initial alkoxide concentration results in the formation of bigger particles.

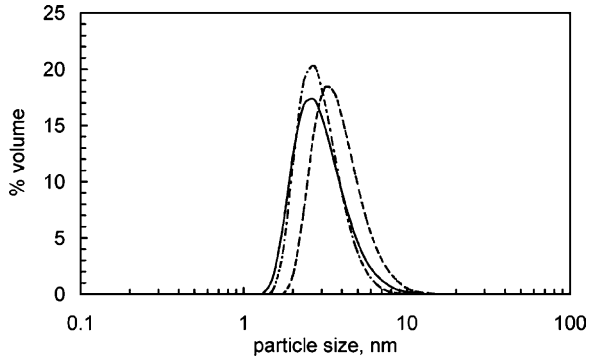

Fig. 2. Volume particle size distributions of titanium dioxide particles synthesized under the following operating conditions $c_{Ti} = 1$ mol/l, $W = 2$, $H = 0.25$, and FR = 220 ml/min; the three lines correspond to three different measurements carried out on three different samples prepared under the same synthesis conditions.

This is probably related to the fact that higher reactant concentrations favour, in this concentration range, the growth of particles rather than the nucleation of new ones. Also the hydrolysis ratio (W) has the same effect (result not shown here); in fact, the formed particles get bigger as the hydrolysis ratio is increased, when the other parameters are kept at their original values.

The hydrochloric acid content, quantified in this work by the H value, has little effect on the initial mean particle size. In fact, comparison of PSDs of titanium dioxide particles obtained at different H values, showed very similar results. However, a tremendous effect was detected on particle stability. In fact, as it is clear from Fig. 4

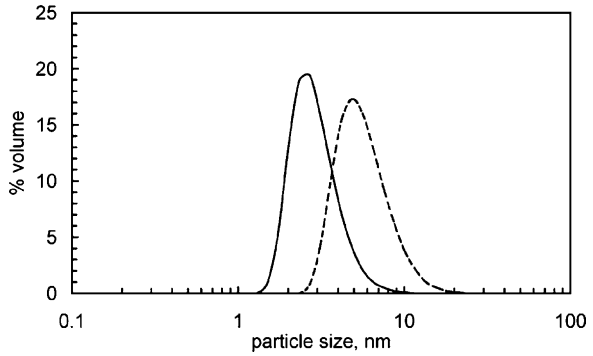

Fig. 3. Volume particle size distributions of titanium dioxide particles synthesized for $H = 0.25$, $W = 2$, FR = 110 ml/min and $c_{Ti} = 0.1$ mol/l (continuous line) and $c_{Ti} = 1$ mol/l (dashed line).

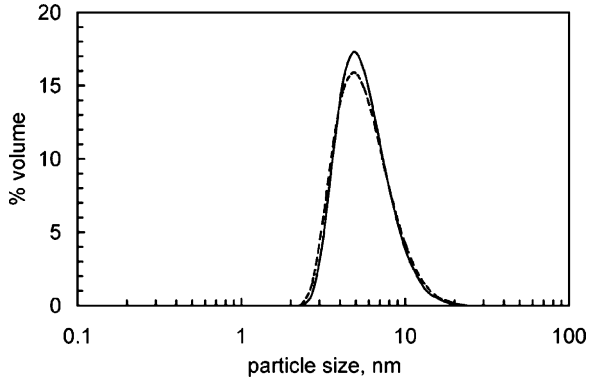

Fig. 4. Volume particle size distributions of titanium dioxide particles synthesized for $H = 0.5$, $W = 2$, FR = 110 ml/min, $c_{Ti} = 1$ mol/l as soon as synthesized (continuous line) and after four days or gentle stirring (dashed line).

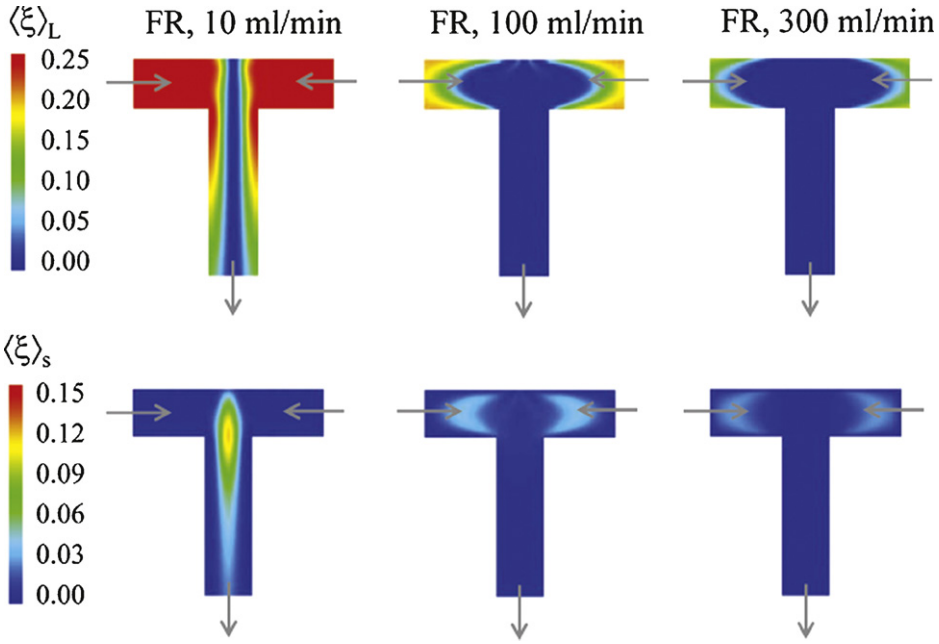

Fig. 5. Contour plots for the large-scale variance (top) and small-scale variance (bottom) at different FR values.

the PSD of titanium dioxide particles synthesized at high H values (e.g., $H = 0.5$) remains constant and after four days it was identical to what originally measured. When the H factor is lowered down to 0.25, and therefore less acid is available, aggregation becomes very important, and the mean particle size increases with time. The effect of the hydrochloric acid content is usually related to the ability of solid oxides to form in aqueous suspensions electrical charges. These charges are caused by the amphoteric dissociation of surface hydroxyl groups, the adsorption of protons and hydroxyl ions, or metal hydroxo compounds from the hydrolysis of solid material. The strong repulsive force among charged particles reduces the probability to aggregate and therefore more stable sols can be formed in acidic or alkaline media.

The effect of these operating parameters (i.e., c_{Ti}, W, H) during particle synthesis have been extensively investigated in the past and our results are consistent with similar works published and available in the specialized literature [44]. However, as already reported the effect of mixing has received little or no attention. For this reason it is particularly interesting to analyse the effect of this parameter on the final PSD of synthesized particles. Mixing can be quantitatively manipulated in the Vortex Reactor simply changing the flow rates of the inlet solutions.

As already reported in the previous section mixing can be quantified by the local value of the large- and small-scale variances. The contour plots of these quantities for the different flow rates investigated in this work are reported in Fig. 5. As expected the large-scale variance reaches its maximum value in the inlets and is then destroyed by turbulence. Due to the fact that mixing is a cascade process, the small-scale variance is generated in the regions where the large-scale variance is dissipated, and is instead dissipated afterwards due to molecular mixing. It is interesting to point out that the regions of the reactor presenting high values of large-scale variance are sensibly reduced as the flow rate is increased. Moreover, it is also clearly evident that at low flow rates at the outlet some macro-scale gradients are still present. The situation improves when the flow rate is increased, reducing the regions of the reactor characterized by macro- and micro-scale gradients.

This is confirmed by the calculations of the volume-averaged mixing times throughout the entire reactor reported in Fig. 6. In this

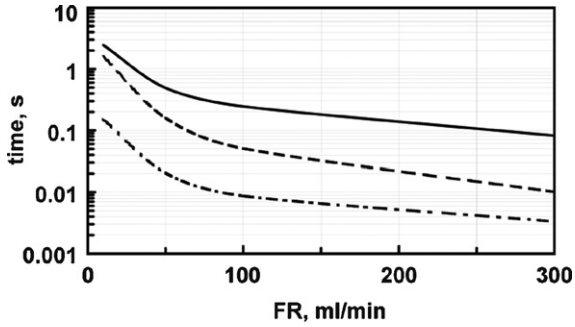

Fig. 6. Mean residence time (continuous line), macro-mixing time (dashed line) and micro-mixing time (dashed–dotted line) versus the reactor flow rate (FR).

figure for the different flow rates investigated, the relevant characteristic times are reported, namely, the mean residence time of the reactants in the reactor, and the macro- and micro-mixing times. As expected increasing the flow rate all these characteristic times are sensibly reduced. However, at low flow rates, the time required for the reactant solutions to mix down to the molecular level is quite large and very similar to the mean residence time of the reactor, resulting in very poor mixing and macro- and micro-scale segregation still characterizing the fluids leaving the reactor outlet. At higher flow rates the mixing time is much smaller than the residence time, and therefore when the fluid leaves the reactor it is completely mixed at the macro- and micro-scale levels.

Fig. 7 compares the PSD obtained at the minimum and the maximum flow rate investigated in this work. As it is possible to see the effect is quite important, since increasing the flow rate from 3 to 330 ml/min the resulting PSD is totally different. For the lowest flow rate the PSD is very broad, and particles as big as 70 nm are produced, whereas for the higher flow rate particles are much smaller, and the PSD has as higher bound 8 nm. As already mentioned the effect of these operating parameter has been carefully investigated, and a summary is reported in Fig. 8. As it is seen, there is a steady decrease of the mean particle size as the flow rate is increased (and as mixing becomes more and more efficient) until a constant value

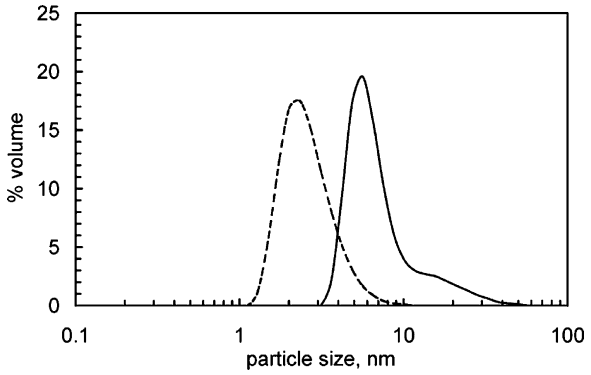

Fig. 7. Volume particle size distributions of titanium dioxide particles synthesized for $c_{Ti} = 1.0$ mol/l, $W = 2$, $H = 0.25$, and for FR = 3 ml/min (continuous line) and for FR = 330 ml/min (dashed line).

is reached. This decrease is caused by the fact that better mixing favours nucleation of new particles with respect to particle growth until a constant value is reached. In fact, as soon as the characteristic mixing time becomes smaller than the typical particle formation time, a further improvement in mixing does not affect any more the final PSD. For the operating conditions reported in Fig. 8 this characteristic particle formation time is about 0.03 s, corresponding to FR ≈ 200 ml/min.

It is also interesting to point out that if the effect of mixing is significant on the PSD of titanium dioxide particles as soon as synthesized, its effect is even greater in terms of their time evolution. In Fig. 9 the time evolution of two different samples prepared under that same operating conditions but at different flow rates are reported. As it is possible to see when particles are synthesized at high flow rate, their initial particle size is very small, and their hydrolysed state is such that they tend to be stable and do not show any tendency to aggregate, whereas on the opposite when the flow rate is very small (and mixing is poor), particles are bigger and tend to aggregate forming bigger particles and eventually under some operating conditions form an aggregate of infinite size called gel.

SEM and FESEM observation supported the hypothesis that under these operating conditions two distinct steps exist. In the first step a burst of particles is produced by nucleation in a very short time. Then this sol evolves into different products through aggregation. In fact the filtered and dried powders observed at the microscope (see Fig. 10) showed a structure resembling that of large aggregates formed by very small primary particles, with about the same PSD of the particles analysed immediately after hydrolysis. This is also supported by specific surface area measurements not reported in this work for the sake of brevity.

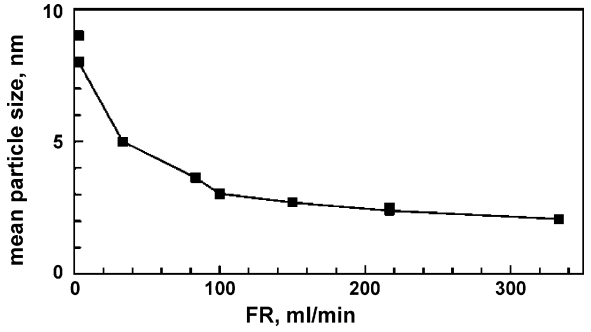

Fig. 8. Mean particle size for titanium dioxide particles synthesized for $H = 0.25$, $W = 2$, $c_{Ti} = 1.0$ mol/l at different FR values.

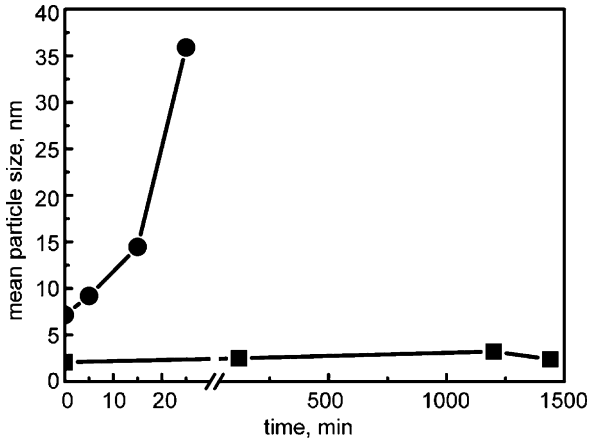

Fig. 9. Time evolution of the mean particle size of titanium dioxide particles synthesized for $c_{Ti} = 1$ mol/l, $W = 2$, $H = 0.25$ at FR = 3 ml/min (circles) and FR = 330 ml/min (squares).

If for the different cases investigated the total particle number density is plotted versus time (see for example Figs. 11 and 12) it is possible to observe the linear decay predicted by Eq. (11). As previously highlighted, the slope characterizing the decay of the total particle number density, is function of a kinetic constant k_0, of the initial titanium concentration c_{Ti} and of the residual water concentration after hydrolysis c_W that can be easily calculated as follows:

$$c_W = c_W^0 - H_0 c_{Ti}, \tag{12}$$

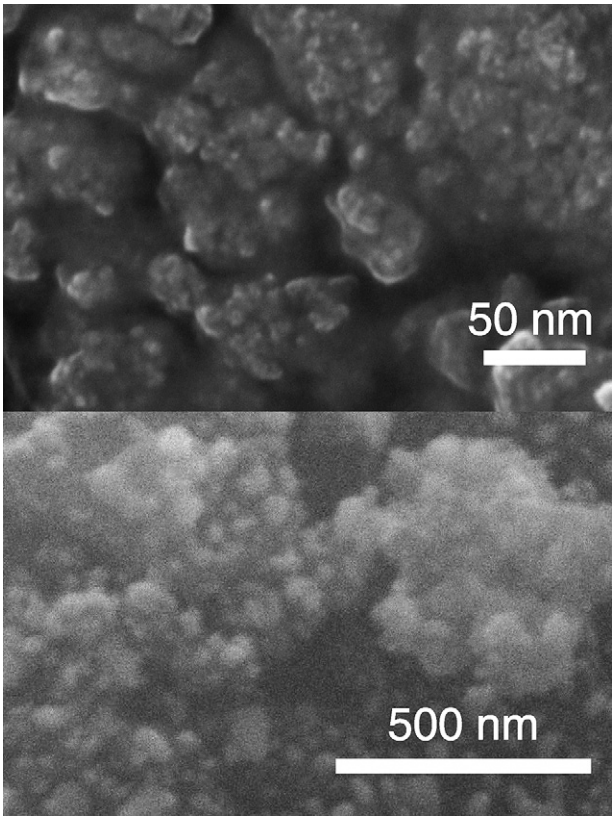

Fig. 10. Morphology of titanium dioxide aggregates synthesized for $c_{Ti} = 1$ mol/l, $W = 2$, FR = 110 ml/min and for $H = 0.25$ (top) and $H = 0.5$ (bottom).

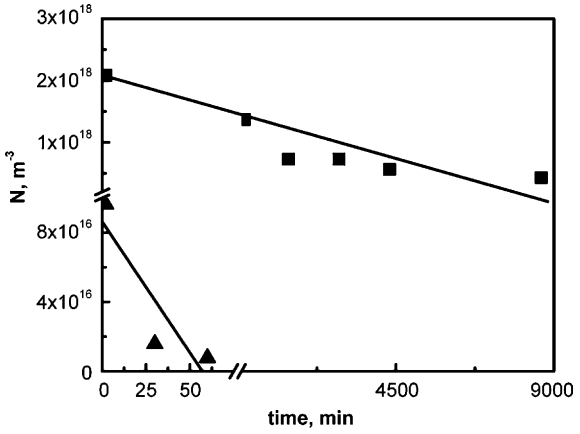

Fig. 11. Time evolution of the total particle number density (N) for $c_{Ti} = 0.5$ mol/l, $H = 0.5$, FR = 110 ml/min; $W = 4$ (triangles) and $W = 2$ (squares).

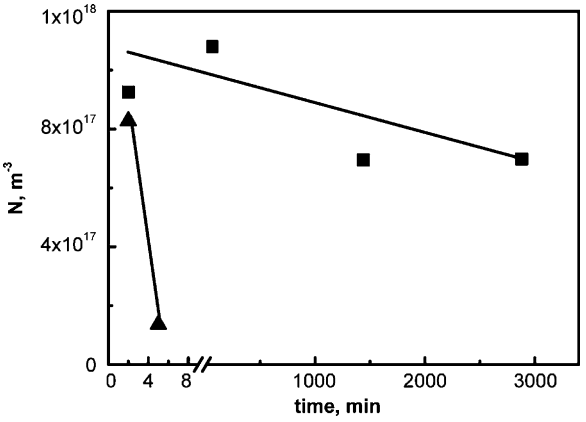

Fig. 12. Time evolution of the total particle number density (N) for $c_{Ti} = 0.5$ mol/l, $H = 0.25$, FR = 110 ml/min; $W = 4$ (triangles) and $W = 2$ (squares).

where c_W^0 is the initial water concentration, and $H_0 = 1.46$ is the average amount of water consumed immediately after hydrolysis in the first stages of particle formation; k_0 is therefore a kinetic constant that does not depend on titanium alkoxide and water concentrations, but only on the tendency of the primary particles to stick together and aggregate, namely for this particular case the hydrochloric acid content. If for $H = 0.5$ all the slopes from the different time evolutions are calculated a unique value

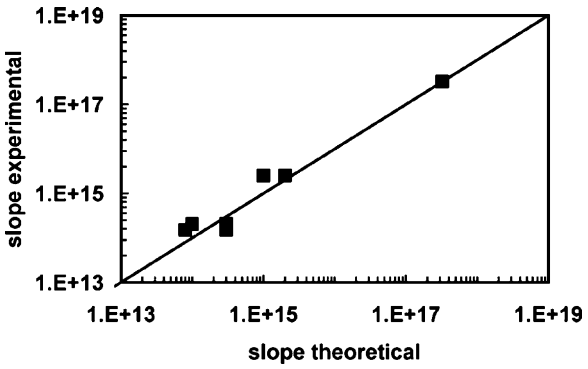

Fig. 13. Comparison between the experimental and calculated slope for the time evolution of total particle number density for all the investigated operating conditions and for $H = 0.5$.

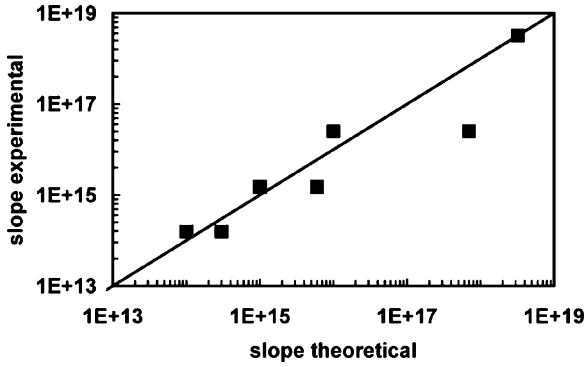

Fig. 14. Comparison between the experimental and calculated slope for the time evolution of total particle number density for all the investigated operating conditions and for $H = 0.25$.

of the kinetic constant that can fit all the experimental data is found. In Fig. 13 the comparison of the calculated and experimental slope for $k_0 = 6 \times 10^{15}$ and $p = 5$ is reported, and as it can be seen the agreement is satisfactory. In Fig. 14 the same comparison is reported for $H = 0.25$, resulting in this case in a bigger kinetic constant value $k_0 = 6 \times 10^{16}$ and $p = 5$; in fact, as previously observed the smaller is the acid content the faster is the aggregation process. It is also worth noticing that the value $p = 5$ is supported by other investigations [40], and can be obtained only if $n = 3$ and $k = 2$. In other words this result implies that adhesion between particles requires the condensation between three hydroxyl groups on each particle, with the second step being the kinetically limiting one (irreversible) and the others being at equilibrium.

These results confirm that during condensation particle aggregation is in the so-called reaction limited regime and therefore its rate is only affected by reactant concentrations as explained in Eq. (11). Nevertheless, it is worth reminding that the effect of mixing is still very important because it determines the initial particle size of the primary particles. Small differences in the primary particle size result in order of magnitudes of difference in the total particle number density, resulting therefore in very different time evolutions, but same kinetic constants.

5. Conclusions

In this work the production of titanium dioxide nanoparticles via the sol–gel route in a Vortex Reactor was considered. The main novelty of this work stands in the investigation of the effect of many operating parameters during synthesis including the mixing rate of the reactants. This investigation was carried out quantitatively by adopting a special passive mixer, whose characteristic mixing features can be easily tuned by manipulating the flow rate of the reactants. This analysis is supported by detailed CFD simulations of the velocity and turbulent fields in the reactor at the different operating conditions investigated.

The reported results clearly show that mixing plays a very important role: not only it determines the PSD of the particles formed immediately after mixing, but it affects also its subsequent evolution. In fact, as demonstrated by the theoretical analysis carried out in this work, after synthesis particles aggregate in the so-called reaction limited regime, but still since mixing determines the size, the number density and the hydrolysed state of the primary particles, it indirectly affects also the aggregation/condensation process.

The results seem to support that mixing can be actively used as one of the operating parameters during synthesis, rather than be passively accepted as a characteristic of the reactor adopted for particle synthesis. The use of adaptable mixing devices, such as the one described in this work, allows to tune the mixing rate in order to obtain the particulate product (e.g., sol or gel) with the desired particle size and morphology. Moreover, it should be highlighted that the CFD calculations, for the global mixing time-scale reported in this work, can be effectively used during process scale up. In fact, as showed in our previous work for precipitation and crystallization [36], a few selected experiments in one equipment (performed under different mixing rates) and CFD calculations of the characteristic time-scale of mixing, suffice to scale up the particle formation process. In fact, for the identical chemical recipe, the same particulate product is obtained in different reactors, if both reactors are operated under the same mixing conditions. The mixing conditions can be considered identical if the global mixing time, calculated with Eq. (7), is the same. Because, as showed with the experimental evidence reported in this work, the effect of mixing on this sol–gel process is very similar to that on standard precipitation, we can extend this scale up methodology to sol–gel processes.

Acknowledgement

This research project has been partially supported by the CRT foundation through the Lagrange project.

Appendix A. Supplementary data

Supplementary data associated with this article can be found, in the online version, at doi:10.1016/j.cej.2008.10.031.

Appendix B. Supplementary data

References

[1] N.S. Allen, M. Edge, A. Ortega, C.M. Liauw, J. Stratton, R.B. McIntyre, Behaviour of nanoparticle (ultrafine) titanium dioxide pigments and stabilizers on the photooxidative stability of water based acrylic and iscocyanate based acrylic coatings, Polymer Degrad. Stabil. 78 (2002) 467–478.
[2] K. Hasimoto, H. Irier, A. Fujishima, TiO_2photocatalysis: a hystorical overview and future prospects, Jpn. J. Appl. Phys. 44 (2005) 8268–8301.
[3] A. Fujishima, T.N. Rao, D.A. Tryk, Titanium dioxide photocatalysis, J. Photochem. Photobiol. C 1 (2000) 1–21.
[4] G.-M. Zuo, Z.-X. Cheng, H. Chen, G.-W. Li, T. Miao, Study of photocatalytic degradation of several volatile organic compounds, J. Hazard. Mater. B 128 (2006) 158–163.
[5] A.L. Linsebigler, G.Q. Lu, J.T. Yates, Photocatalysis on TiO_2 surfaces-Principles, mechanisms, and selected results, Chem. Rev. 95 (1995) 735–758.
[6] S.S. Watson, D. Beydoun, J.A. Scott, R. Amal R, The effect of preparation method on the photoactivity of crystalline titanium dioxide particles, Chem. Eng. J. 95 (2003) 213–220.
[7] A. Mills, N. Elliott, G. Hill, D. Fallis, J.R. Durrant, R.L. Willis, Preparation and characterisation of novel thick sol–gel titania film photocatalysts, Photochem. Photobiol. Sci. 2 (2003) 591–596.
[8] M.H. Habibi, H. Vosooghian, Photocatalytic degradation of some organic sulfides as environmental pollutants using titanium dioxide suspension, J. Photochem. Photobiol. A 174 (2005) 45–52.
[9] R.R. Bacsa, J. Kiwi, Effect of rutile phase on the photocatalytic properties of nanocrystalline titania during the degradation of p-coumaric acid, Appl. Cat. B 16 (1998) 19–29.
[10] J.M. Watson, A.T. Cooper, J.R.V. Flora, Nanoglued titanium dioxide aerogels for photocatalysis, Env. Eng. Sci. 22 (2005) 666–675.
[11] M.C. Yan, F. Chen, J.L. Zhang, M. Anpo, Preparation of controllable crystalline titania and study on the photocatalytic properties, J. Phys. Chem. B 109 (2005) 8673–8678.
[12] A. Testino, I.R. Bellobono, V. Buscaglia, C. Canevali, M. D'Arienzo, S. Polizzi, R. Scotti, F. Morazzoni, Optimizing the photocatalytic properties of hydrothermal TiO_2 by the control of phase composition and particle morphology. A systematic approach, J. Am. Chem. Soc. 129 (2007) 3564–3575.
[13] R. Scotti, I.R. Bellobono, C. Canevali, C. Cannas, M. Catti, M. DArienzo, A. Musinu, S. Polizzi, M. Sommariva, A. Testino, F. Morazzoni, Sol–gel pure and mixed-phase titanium dioxide for photocatalytic purposes: relations between phase composition, catalytic activity, and charge-trapped Sites, Chem. Mat. 20 (2008) 4051–4061.
[14] C. Su, B.-Y. Hong, C.-M. Tseng, Sol–gel preparation and photocatalysis of titanium dioxide, Catal. Today 96 (2006) 119–126.
[15] M. Lackhoff, X. Prieto, N. Nestle, F. Dehn, R. Niessner, Photocatalytic activity of semiconductor-modified cement—influence of semiconductor type and cement ageing, Appl. Catal. B 43 (2003) 205–216.
[16] M. Keshmiri, T. Troczynski, M. Mohseni, Oxidation of gas phase trichloroethylene and toluene using composite sol–gel TiO_2 photocatalytic coatings, J. Hazard. Mater. B 128 (2006) 130–137.
[17] A. Petrella, M. Tamborra, P.D. Cozzoli, M.L. Curri, M. Striccoli, P. Cosma, G.M. Farinola, F. Babudri, F. Naso, A. Agostiano, TiO_2 nanocrystals—MEHPPV composite thin films as photoactive material, Thin Solid Films 451–452 (2004) 64–68.
[18] P.M. Ajayan, L.S. Schadler, P.V. Braun, Nanocomposite Science and Technology, Wiley-VCH, Weinheim, 2003.
[19] S.E. Pratsinis, Flame aerosol synthesis of ceramic powders, Prog. Energy Combust. Sci. 24 (1998) 197–219.
[20] Y.V. Kolen'ko, V.D. Maximov, A.A. Burukhin, V.A. Muhanov, B.R. Churagulov, Synthesis of ZrO_2 and TiO_2 nanocrystalline powders by hydrothermal process, Mater. Sci. Eng. C 23 (2003) 1003–1038.
[21] Z. Li, B. Hou, Y. Xu, D. Wu, Y. Sun, W. Hu, F. Deng, Comparative study of sol–gel hydrothermal and sol–gel synthesis of titania–silica composite nanoparticles, J. Solid State Chem. 178 (2005) 1395–1405.
[22] F. Sayilkan, M. Asilturk, S. Erdemoglu, M. Akarsu, H. Sayilkan, M. Erdemoglu, E. Arpac, Characterization and photocatalytic properties of TiO_2-nanosols synthetized by hydrothermal process at low temperature, Mater. Lett. 60 (2006) 230–235.
[23] J. Yang, S. Mei, M.F. Ferreira, Hydrothermal processing of nanocrystalline anatase films from tetraethylammonium hydroxide peptized titania sols, J. Eur. Ceram. Soc. 24 (2004) 335–339.
[24] X.-Z. Ding, X.-H. Liu, Synthesis and microstructure control of nanocrystalline titania powders via sol–gel process, Mater. Sci. Eng. A 224 (1997) 210–215.
[25] C.W. Turner, Sol–gel process—principles and applications, Ceram. Bull. 70 (1998) 1487–1490.
[26] M.T. Harris, H. Byers, Effect of solvent on the homogeneous precipitation of titania by titanium ethoxide hydrolysis, J. Non-Cryst. Solids 103 (1998) 49–64.
[27] J. Blanchard, F. Ribot, C. Sanchez, P.-V. Bellot, A. Trokiner, Structural characterization of titanium-oxo-polymers synthesized in the presence of protons or complexing ligands as inhibitors, J. Non-Cryst. Solids 265 (2000) 83–97.
[28] C.J. Brinker, G.W. Scherer, Sol–Gel Science—The Physics and Chemistry of Sol–Gel Processing, Academic Press, San Diego, 1990.
[29] K.Y. Jung, S.B. Park, M. Anpo, Photoluminescence and photoactivity of titania particles prepared by the sol–gel technique: the effect of the calcination temperature, J. Photochem. Photobiol. A 170 (2005) 247–252.
[30] R.O. Fox, Computational Models for Turbulent Reacting Flows, Cambridge University Press, Cambridge, 2003.
[31] B.K. Johnson, R.K. Prud'homme, Chemical processing and micromixing in confined impinging jets, AIChE J. 49 (2003) 2264–2282.
[32] Y. Liu, R.O. Fox, CFD predictions for chemical processing in a confined impinging-jets reactor, AIChE J. 52 (2006) 731–744.
[33] E. Gavi, D.L. Marchisio, A.A. Barresi, CFD modelling and scale-up of Confined Impinging Jet Reactors, Chem. Eng. Sci. 62 (2007) 2228–2241.
[34] A. Soloviev, B. Ivanov, R. Tufeu, A.V. Kanaev, Nanoparticle growth during the induction period of the sol–gel process, J. Mater. Sci. Lett. 20 (2001) 905–906.
[35] D.L. Marchisio, M. Soos, J. Sefcik, M. Morbidelli, Role of turbulent shear rate distribution in aggregation and breakage processes, AIChE J. 52 (2006) 158–173.
[36] D.L. Marchisio, L. Rivautella, A.A. Barresi, Design and scale-up of chemical reactors for nanoparticle precipitation, AIChE J. 52 (2006) 1877–1887.
[37] E. Gavi, D.L. Marchisio, A.A. Barresi, On the importance of mixing for the production of nano-particles, J. Disp. Sci. Tech. 29 (2008) 548–554.
[38] F. Lince, D.L. Marchisio, A.A. Barresi, Strategies to control the particle size distribution of poly-caprolactone nanoparticles for pharmaceutical applications, J. Coll. Int. Sci. 332 (2008) 505–515.
[39] E. Gavi, L. Rivautella, D.L. Marchisio, M. Vanni, A.A. Barresi, G. Baldi, CFD modelling of nano-particle precipitation in Confined Impinging Jet Reactors, Chem. Eng. Res. Dev. 85 (A5) (2007) 735–744.
[40] M. Rivallin, M. Benmami, A. Kanaev, A. Gaunand, Sol–gel reactor with rapid micromixing. Modelling and measurements of titanium dioxide nano-particle growth, Chem. Eng. Res. Des. 83 (A1) (2005) 67–74.
[41] M.Z. Smoluchowski, Versuch Einer Mathematischen Theorie Der Koagulationskinetik Kolloider Losunger, Z. Phys. Chem. 92 (1917) 129–145.
[42] M. Soos, D.L. Marchisio, J. Sefcik, R.O. Fox, M. Morbidelli, Assessment of gel formation conditions in turbulent jets, in: Proceedings of the Fifth World Congress on Particle Technology, Orlando, FL, USA, April 23–27, 2006.
[43] D.L. Marchisio, M. Soos, J. Sefcik, M. Morbidelli, A.A. Barresi, G. Baldi, Effect of fluid dynamics on particle size distribution in particulate processes, Chem. Eng. Technol. 29 (2006) 191–199.
[44] D.L. Marchisio, F. Omegna, A.A. Barresi, P. Bowen, Effect of mixing and other operating parameters in sol–gel processes, Ind. Eng. Chem. Res. 47 (2008) 7202–7210.

[45] Y. Liu, C.Y. Cheng, Y. Liu, R.K. Prud'homme, R.O. Fox, Mixing in a multi-inlet vortex mixer (MIVM) for flash nano-precipitation, Chem. Eng. Sci. 63 (2008) 2829–2842.
[46] B.K. Johnson, Flash nanoprecipitation of organic actives via confined micromixing and block co-polymer stabilization, PhD Thesis, Princeton University, (2003).
[47] S. Valerio, M. Vanni, A.A. Barresi, G. Baldi, Engineering modelling of turbulent flows in chemical engineering applications, Trends Chem. Eng. 5 (1998) 1–44.
[48] A. Soloviev, R. Tufeu, C. Sanchez, A. Kanaev, Nucleation stage in the $Ti(OPri)_4$ sol–gel process, J. Phys. Chem. B 105 (2001) 4175–4180.